



### **Science Arts & Métiers (SAM)**

is an open access repository that collects the work of Arts et Métiers Institute of Technology researchers and makes it freely available over the web where possible.

This is an author-deposited version published in: <https://sam.ensam.eu>  
Handle ID: <http://hdl.handle.net/10985/22815>

#### **To cite this version :**


Matthew SLEIGHT, Laurent PELTIER, Boris PIOTROWSKI, Fodil MERAGHNI - Design, Characterization, and Finite-Element Optimization of a Two-Way Assisted Through SuperElasticity Torsion Actuator - Shape Memory and Superelasticity - 2022

Any correspondence concerning this service should be sent to the repository

Administrator : [scienceouverte@ensam.eu](mailto:scienceouverte@ensam.eu)



# Design, Characterization, and Finite-Element Optimization of a Two-Way Assisted Through SuperElasticity Torsion Actuator

Matthew Sleight<sup>1</sup> · Laurent Peltier<sup>1</sup> · Boris Piotrowski<sup>1</sup> · Fodil Meraghni<sup>1</sup> 

**Abstract** The present study aims at developing a new Shape Memory Alloy (SMA) autonomous torsion actuator that exhibits Two-Way reversible memory effect Assisted by SuperElasticity. The developed actuator noted hereafter TWASE is composed by a single NiTi compact component having two distinct SMAs parts on one single axis: a SuperElastic part (length  $L_{SE}$ ) and a Shape Memory Effect part (length  $L_{SME}$ ). The proposed design ensures twisting the actuator when heated, this activates then the superelastic part putting back the actuator into its original shape as a result of a decrease in temperature. Hence, the actuator moves and goes back to the initial position autonomously (self-reversible). It has been established that the actuation efficiency is strongly dependent on the length ratio ( $\lambda_{SME}$ ) of the SME part with respect to the total length of the torsion actuator. Experimentally, an actuator with a length ratio of 3/5 has been developed and tested. The actuator's axis is subjected to a specific heat treatment for obtaining a SMA wire with two distinct zones. A FE analysis using a proper UMAT subroutine into Abaqus software has been performed to predict the kinematics and the thermomechanical response of the actuator and finally to optimize it accordingly. The developed computational

model captures the actuator responses and the subsequent optimizations are carried out leading to the improved specifications, which are confirmed experimentally. The experimental validation has been carried out using a prototype set-up of a torsion bench built by 3D printing. The actuation response of TWASE is numerically analyzed for several length ratio configurations. Based on the numerical simulations, the performance of the actuator has been optimized in terms of rotation angle and length ratio. The best ratio of shape memory to superelastic parts in the actuator has been predicted to 1/4 for obtaining the expected two-way reversible memory effect (TWASE).

**Keywords** Shape memory alloy · Two-way shape memory effect · Finite element analysis · Actuator design · Actuation optimization

## Introduction

SMA actuators provide an excellent technological opportunity to replace conventional heavier and more complex actuators such as electric motors, pneumatics, and hydraulics [1–3]. They react directly to environmental stimuli such as temperature inducing phase transformation and consequently develop an actuation force [4], and thus they do not require an external mechanism. These low weight SMA actuators have been used in many industries [5–11] either as one-use actuators or assisted by a second component to permit the resetting through reverse phase transformation. In the same way, other kinds of actuators have been used such as wax actuators and bimetallic actuators. Wax actuators have the advantage of being able to provide great energy but present a heavy weight and need extra components to create an angular reaction. They

This invited article is part of a special issue of *Shape Memory and Superelasticity* honoring Etienne Patoor for his contributions to the field of phase transforming materials and shape memory alloys. The special issue was organized by Dr. Fodil Meraghni, Ecole Nationale Supérieure d'Arts et Métiers (Arts et Métiers Institute of Technology), and Dr. Dimitris Lagoudas, Texas A&M University.

✉ Fodil Meraghni  
fodil.meraghni@ensam.eu

<sup>1</sup> Arts et Métiers Institut of Technology, CNRS, Université de Lorraine, LEM3-UMR 7239, 57000 Metz, France

also lack reactivity because the wax producing the force needs to melt [7]. The bimetallic actuator gives an angular response and is also reversible. Consequently, it is frequently used as an actuator, but it does not provide a great strength and its deformation is linear with respect to the temperature [8], which means it does not just react at the temperatures required but at every temperature. SMA actuators provide many advantages over other actuators such as the steady-stable thermally activated response, and more energy produced per cubic meter. For instance, the NiTi SMA displays one of the highest work densities at  $10 \text{ J/cm}^3$ , which is 25 times greater than the work density of electric motors [11] and is able to move more than 100 times its weight [1, 3].

However, one limitation of the SMA actuators resides in their capability to reset the actuator. Indeed, SMAs exhibit the characteristics to provide TWME (Two Way Memory Effect) limited to very low stress levels, which are unsuitable for actuation applications [12, 13]. A first solution can disassemble the mechanism to replace the actuator (one shot) or reset through, for example, a compression device. This solution is expensive and may not be compatible for industrial applications. A second solution is to reset the actuator with an external force through another component, such as a spring [1, 6]. The memory element generates motion to overcome a resistant force during heating, and the actuator is reset upon cooling. It has been applied on automotive applications through a temperature-sensitive controller valve, which controls the shifting pressure in automatic transmissions [4]. In this case, the NiTi SMA spring and the steel one are in opposition. At low temperatures, the force of the steel spring is higher than that of the SMA spring, in the martensitic state. The moveable piston of the valve is also pushed into the 'closed' position for this particular application. When the temperature of the transmission and the transmission fluid increases to operating temperature, the SMA spring in the martensitic state expands, overcoming the steel spring force, and pushing the piston into the 'open' position. This solution with an additional component to reset the actuator induces more complex mechanisms and exhibits poor energy efficiency.

In the present paper, a new SMA torsion actuator which does not need any other component for resetting is developed and analyzed: the TWASE (Two-Way Assisted through SuperElasticity) actuator. The properties of the TWASE actuator are obtained on a one single component thanks an appropriate thermomechanical heat treatment described in the first part of the paper. The  $\text{Ni}_{50}\text{Ti}_{50}$  alloy has been studied since the 1960s. Its shape memory and superelasticity behaviors were discovered fortuitously by Buehler et al. The transformation points of the NiTi alloy can evolve depending on the chemical composition of the

alloy as shown by Frentzel et al. [14] but also as a function of the thermomechanical treatment applied to the alloy [15]. The development of a prototype and this application as an actuator is described to highlight the functionality and its self-reversibility. A Finite-Element model is then proposed to reproduce several cycles of actuation. This numerical model is validated through a comparison with the prototype. It is then applied to optimize the design of the torsion actuator and the thermomechanical treatment to set its response. The simulation is aimed at defining the optimal fraction of SME (Shape Memory Effect) part relative to the SE (superelastic) part so that the actuator could achieve the greatest angle of rotation or displacement. To achieve this, the numerical simulations have been carried out with different SME/SE ratios expressed through the length ratio of the actuator defined in Sect. 2.1. For each numerical experiment, the angle and the corresponding torque values of the actuator are estimated. With those simulations it is possible to determine the right proportion of SME in the actuator and in addition the point on the actuator where the torque and the rotation angle are maximized.

## Shape Memory Alloy and Experimental Methods

### SMA Description, Heat-Treatment, and Actuator Preparation

It is worth reminding that this work aims at developing a new SMA autonomous torsion actuator. The axial geometry of a wire is the most suitable one and ensures the twisting of the actuator. This section is focusing on the thermomechanical analysis of a binary NiTi shape memory alloy wire provided by the company Nimesis Technology (NiTi 50.8 at.%). The "As Received" (AR) state is subjected to specific heat treatments to obtain a dual-zone actuator. To this end, a home-made oven has been designed with two differentiated heating zones allowing a simultaneous double heat treatment of a unique NiTi alloy wire. The heat treatment is applied according to two successive steps. The first step consists in a heat treatment of the whole SMA mono wire at a temperature of  $850^\circ\text{C}$  during 15 min. This step confers to the mono wire an austenitic state with a superelastic (SE) behavior at room temperature. During the second step, the mono wire is treated on a partial length. This second step consists in precipitation at  $380^\circ\text{C}$  during 60 min.

These two thermal treatments provide to the actuator an original property of a SE-assisted two-way actuator (TWASE). In fact, at room temperature, one part of the actuator is martensitic and generates the shape memory effect (SME part), illustrated by the blue part in Fig. 1,

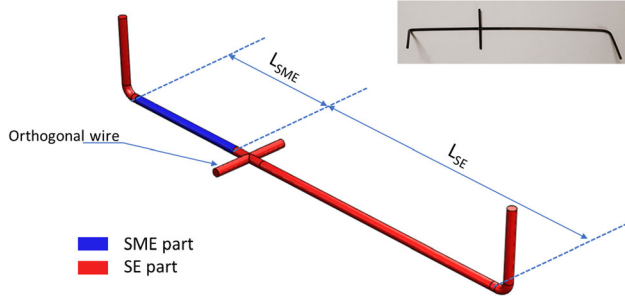


**Fig. 1** Two-Way Assisted through SuperElasticity (TWASE) torsion actuator after being armed. The main axis of the actuator has a constant diameter and it is composed of a SME part (blue) having a length ( $L_{SME}$ ) and a SE part (red) with a length ( $L_{SE}$ ). The small orthogonal axis is placed between them to transmit the torque to the rotating system (transmission axis). The top-right corner image illustrates the actual developed torsion actuator (Color figure online)

while the other part of the actuator, presented in red (Fig. 1), is austenitic and it exhibits a superelastic response.

The mono wire torsion actuator is thus constituted by a longitudinal single axis composed of two distinct parts. The SME part ensures the memory effect actuation and has a length  $L_{SME}$ , whereas the SE part (length  $L_{SE}$ ) serves as a back spring during the re-arming of the two-way actuator.

At this stage, the length ratio of the SME part with respect to the total length of the actuator ( $L_{Tot}$ ) is introduced. It is noted hereafter ( $\lambda_{SME}$ ) and is defined as follows:

$$\lambda_{SME} = \frac{L_{SME}}{L_{SME} + L_{SE}} = \frac{L_{SME}}{L_{Tot}}$$

A prototype with a length ratio  $\lambda_{SME}$  of 3/5 has been designed and fabricated to demonstrate experimentally the proof of concept of the actuator. This choice is motivated by the industrial requirement to develop an autonomous mono wire actuator with two distinct parts, namely SME and SE, that can reach a maximum rotation angle of 25°. When the temperature rises, the SME part rotates the actuator overcoming the SE part. When the temperature decreases, the martensite in the SME part re-appears leaving the SE part to dominate. The austenite brings about to the actuator a rotation in the opposite direction and takes back the actuator to its initial position. The actuator consists of a 1.2 mm diameter NiTi SMA wire with a total length of 120 mm. The shape of the actuator is obtained by hot bending as shown in Fig. 1. The two ends of the actuator are initially bent at 90° in two different planes.

To transmit the torque in torsion, an orthogonal wire (Fig. 1) made of NiTi alloy (the same as for the actuator) in SE regime is welded to the actuator. A recent study shows that the good laser weldability of NiTi-based SMA can allow using these materials in actuation-based high temperature applications [16]. This transmission axis will

transfer the torque from the actuator to the rotation system. The orthogonal axis is welded at the end of the SE part to avoid any microstructural transformation in the SME part that can be induced by the Thermally Affected Zone (TAZ) due to the welding operation.

The transformation temperatures are very important and must be measured. These four temperatures characterize the beginning of the martensitic transformation ( $M_s$ ), the end of the martensitic transformation ( $M_f$ ), the beginning of the austenitic transformation ( $A_s$ ), and the end of the austenitic transformation ( $A_f$ ). In the present work, these temperatures govern the activation of the SME wire and the rotational movements of the actuator [10]. However, these transformation temperatures are known to be strongly related to the stress state [17] as well as the composition of the SMA [10, 18]. To measure the transformation temperatures of the SME part, Differential Scanning Calorimetry (DSC) tests have been performed according to ASTM-F2004 [19]. The DSC tests are carried out to determine the different transformation temperatures of the NiTi alloy without stress. The cooling and heating rates are identical and equal to 10 K/min. Each test consists of 2 complete cycles of transformation. The thermograms presented in the paper are the second cycles in order not to take into account the effect of the martensite produced during the cutting of the samples. The results of the thermomechanical analysis are shown in Fig. 2. The thermograms of the three states SE, SME, and AR are shown in Fig. 2a, while the transformation point temperatures are listed in Fig. 2b. It shows a large deviation in transformation temperature ranging from the NiTi alloy wire in the AR state, 81 K between  $M_s$  and  $M_f$  and 79 K between  $A_s$  and  $A_f$ . In this state, one can confirm that the NiTi AR alloy is not suitable for use as a single or two-way actuator.

### Operating Steps of the TWASE Actuator

The developed actuator operates according to two main steps is illustrated in Fig. 3. These two steps can be summarized as follows:

- (a) The first step has the objective to arm (to activate) the actuator by positioning it in its initial condition (Fig. 3a). The latter consists of applying a 90° rotation to the extremity located close to the SME actuator part, as shown in Fig. 3b. During this step, the SE part will be partially transformed to martensite (coexistence of both austenite and martensite phase). In addition, the first step generates stress induced martensite (reorientation) in the SME part of the actuator. The extremity will then be clamped as illustrated in Fig. 3c.

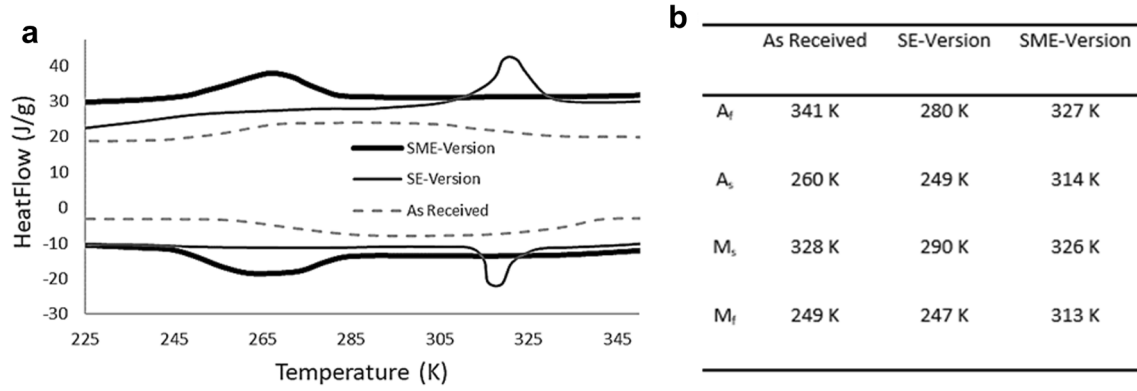


**Fig. 2** Thermomechanical results of the different studied states: **a** DSC thermograms, **b** Transformation temperatures of the three configurations of the studied NiTi SMA Wire

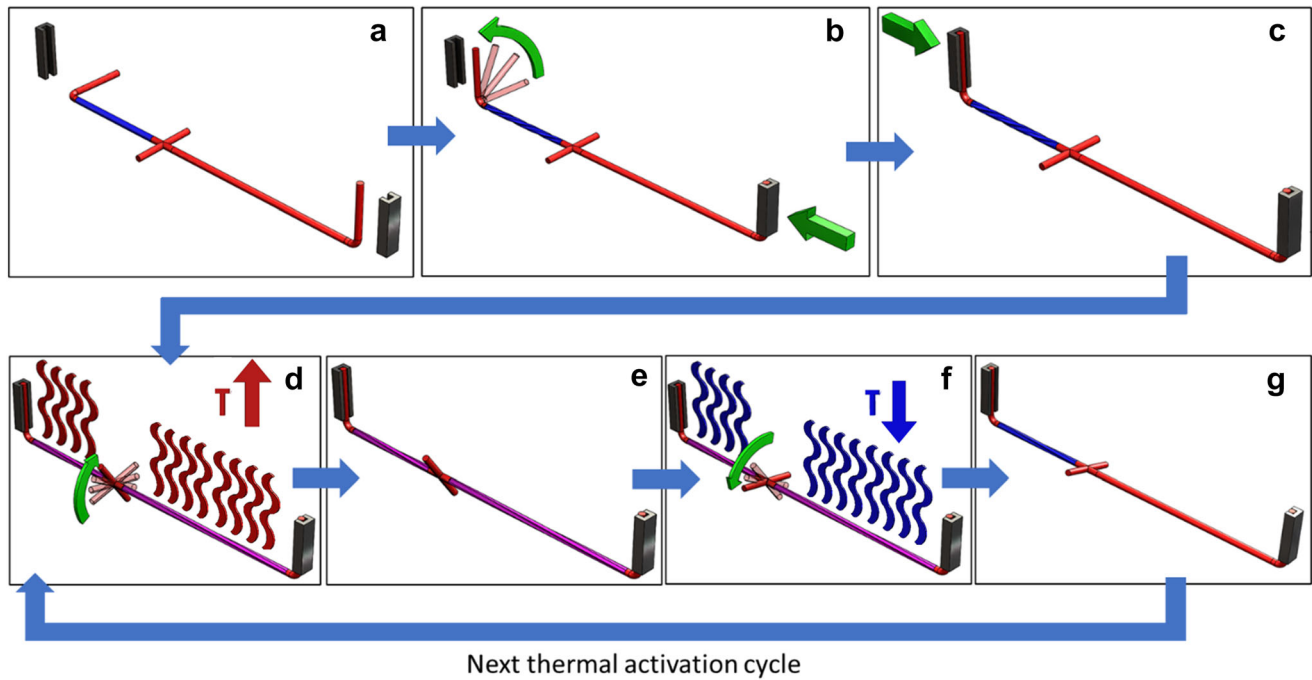


**Fig. 3** Explanation of the TWASE system: **a** As-Build shape (the blue part is martensitic at room temperature, red parts are austenitic at room temperature), **b** placing under the initial torsion stress of the TWASE system, **c** locking of the clamping devices, **d** and **e** arming

the system, **d** first heating of two active parts of the actuator, **e** rotation of actuator due to the reverse phase transformation, **f** progressive cooling of the actuator and **g** ready-to-use system, **f** hot shape of the system, **g** cold shape of the system (Color figure online)

- (b) The second step consists of the TWASE effect allowing the actuation and the two-ways reversible memory effect assisted by superelasticity. This step is controlled by the actuation temperature. One can distinguish two sub-steps that represent an actuation cycle:

- (b-1) An increase of the system's temperature above  $A_s$  induces in the SME part a reverse phase transformation from the reoriented martensite to austenite (Fig. 3d). As a result, the SME part will tend to return to

its initial shape causing the rotation of the whole actuator (Fig. 3e). The SE part will be subjected to the induced twisting torque but it exhibits reversible strain.

- (b-2) A progressive decrease of the system temperature below  $M_f$  brings about progressively the martensitic transformation of the SME part, which is at this stage under the effect of the twisting torque of the SE part. This sub-step is illustrated in Fig. 3f. With the increase of the martensite volume fraction the resistant twisting torque of the



SME part decreases, allowing the actuator to return to its initial configuration under the effect of the SE part, which plays the role of a spring back (Fig. 3g).

The step b with its sub-steps b-1 (figures d and e) and b-2 (figures f and g) can be repeated to achieve the actuation cycles. The cooling and heating rates are identical and equal to 2 K/min.

### Critical Torque Estimation

An experimental device with  $\lambda_{SME}$  of 3/5 has been developed to estimate the critical torque developed by the actuator without any visible deterioration or damage (Fig. 4). The experimental test bench consists of a (i) prototype whose components (wheels and supports) are fabricated by polymer additive manufacturing and (ii) the TWASE single wire torsion actuator as illustrated in Fig. 4c. The experimental procedure aimed at measuring the actuation torque is described in this section. The geometrical model of the experimental device has been achieved using Solidworks 2016, to estimate the torque with a protocol using calibrated masses that generate a force as shown in Fig. 4a and b. The bench test of the TWASE actuator (Fig. 4a) is placed in a thermal oven. To monitor the SMA actuator's response to the thermal stimuli, the experimental device is multi-instrumented in terms of temperature using a thermocouple and in displacement using a linear LVDT sensor.

The device is adjustable to multiple sample sizes since it has the capability to adapt its geometry to any actuator. The actuator is gripped by means of a clamp and its SME causes the rotation of a wheel which is held by supports with ball bearings to limit friction (Fig. 4b). A string is tied

around the wheel and a support is attached to it. Calibrated weights are added to the support. The SMA actuator is subjected to thermal cycles by heating and cooling it. The linear displacement of the plateau is measured by means of the linear transducer (LVDT). The force is increased by adding progressively the masses to the support, the difference in rotation produced during the thermal cycle is measured. With this method, by measuring the angle at which the equilibrium is reached between the actuator's torque and the torque induced by the weights, we can determine the torque after which this angle decreases. Thus, we can determine the evolution of the torque of the actuator with respect to the angle of rotation.

### Numerical Analysis and Simulation

#### Geometrical Modelling

This modelling is aimed at facilitating the subsequent calibration of the model. As a consequence, each geometrical variable of the actuator would be easily adjusted to ensure the requested actuation. The considered shape is the initial one before the arming step. The 120 mm length wire with constant diameter of 1.2 mm is composed of three parts as represented in Fig. 5: (i) the SE part (in red), with a length of 47.5 mm; (ii) the elastic transition part (in white), with 1 mm length; and finally, the SME part (in blue), which has a length of 71.5 mm. The main part, to which the actuating branch is attached, is bent on both sides at 90° in two perpendicular planes. The constitutive law devoted to the SMAs is described in the following section and will be applied on the respective parts of the actuator. For the

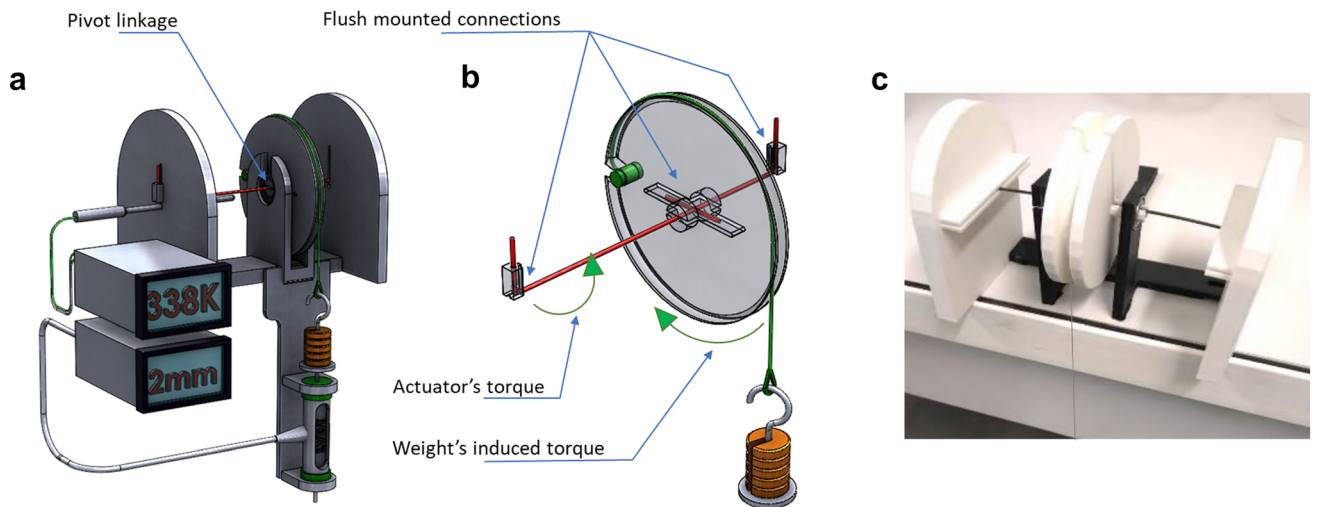


**Fig. 4** Multi-instrumented test bench: **a** Complete version, **b** Focus on the actuator with  $\lambda_{SME}$  of 3/5: (i) a mass is applied, (ii) the TWASE actuator is heated, (iii) the delivered torque can be calculated through

the linear displacement of the LVDT transducer, **c** The actual prototype of the test bench fabricated by polymer additive manufacturing equipped with TWASE single wire torsion actuator

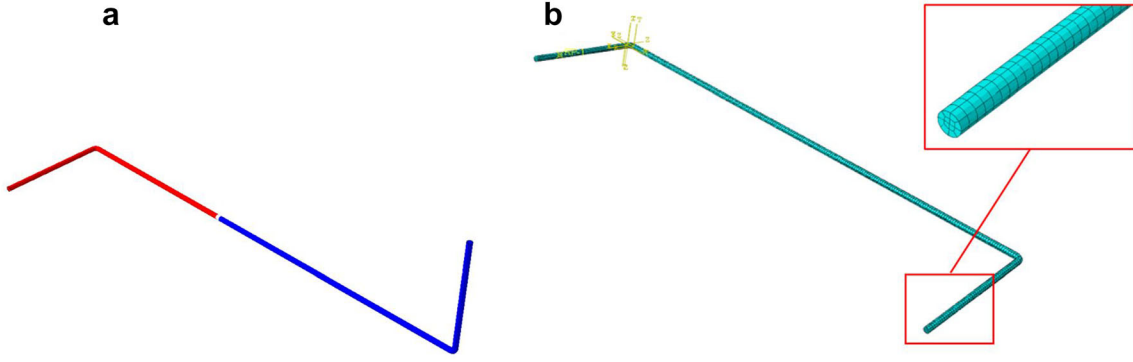


**Fig. 5** **a** Representation of the 3 different zones of the actuator: SE part, frontier zone, SE part **b** Representation of the meshed elements

finite-element analysis, the latter has then been meshed with C3D20 quadratic brick elements (quadratic geometric order) of 0.5 mm length in order to have 4 elements in the thickness, for a total of 3780 elements. A mesh convergence analysis has been performed to ensure that the spatial discretization has no influence on the predicted results. The simulation with 3780 elements induces a time computation of 22 CPU hours on Intel(R) Xeon(R) CPU E5-2630 v3 @ 2.40 GHz. The computations have been conducted on Cassiopee Arts et Métiers Institute of Technology HPC Center.

### SMA Constitutive Behavior

The adopted SMA constitutive behavior has been developed in a previous study [20] and generalized by Chatziathanasiou et al. [21] in a thermodynamical framework. This model has the capability to describe simultaneously the evolution of several strain mechanisms as well as the functional fatigue of SMAs [22, 23]. It has been implemented in the Simcoon [24] mechanical library and is imported in Abaqus Software through a UMAT subroutine. It describes the evolution of the martensite fraction, the forward and the reverse martensite transformation as well as the reorientation of martensite variant under thermo-mechanical loading. Eight internal variables are considered: the strain tensors, the temperature, the martensite volume fraction  $f$  decomposed by Forward and Reverse evolution, the mean transformation strain  $\bar{\epsilon}_{ij}^T$  decomposed by strain orientation due to Forward transformation, Reverse transformation and Reorientation, and the hardening strain for reorientation. The total strain is composed of several contributions describing physical mechanisms, including the elastic strain tensor  $\epsilon_{ij}^e$  and the thermal expansion strain tensor  $\epsilon_{ij}^{th}$ :

$$\epsilon_{ij}^{total} = \epsilon_{ij}^e + \epsilon_{ij}^{th} + \epsilon_{ij}^T$$

A thermodynamic potential is assumed to model polycrystalline SMAs. It corresponds to a macroscopic

expression of the Gibbs free energy variation between an initial austenitic state and a biphasic Martensite–Austenite current one.

$$\begin{aligned} \Delta G(\sigma_{ij}, T, f, \bar{\epsilon}_{ij}^T) = & -\frac{1}{2} \sigma_{ij} S_{ijkl} \sigma_{kl} - \sigma_{ij} \alpha_{ij} \Delta T - \Delta T S^A \\ & + B(T - T_0)f \\ & - \sigma_{ij} \bar{\epsilon}_{ij}^T f + \frac{1}{2} f H_e \bar{\epsilon}_{ij}^T \bar{\epsilon}_{ij}^T + \frac{1}{2} H_f f^2 \end{aligned}$$

$T$  and  $\sigma_{ij}$  are, respectively, the temperature and the Cauchy stress tensor in the RVE,  $S_{ijkl}$ ,  $\alpha_{ij}$ ,  $B$ ,  $S^A$ ,  $T_0$  are, respectively, the matrix compliance tensor, the matrix thermal expansion tensor, the parameter describing the transformation temperatures variation with stress level, the austenitic entropy and the equilibrium temperature.  $H_e$  and  $H_f$  are two parameters characterizing in a global way incompatibility between grains and between variants.

From this expression, thermodynamics forces (transformation, orientation, entropic and elastic) associated to each variable are derived.

$$F_f = -\frac{\delta(\Delta G)}{\delta f} = -B(T - T_0) + \sigma_{ij} \bar{\epsilon}_{ij}^T - H_f f - \frac{1}{2} H_e \bar{\epsilon}_{ij}^T \bar{\epsilon}_{ij}^T$$

$$f F_{\bar{\epsilon}_{ij}^T} = -\frac{\delta(\Delta G)}{\delta \bar{\epsilon}_{ij}^T} = f \left( \sigma_{ij}^D - H_e \bar{\epsilon}_{ij}^T \right)$$

$$F_T = -\frac{\delta(\Delta G)}{\delta T} = \sigma_{ij} \alpha_{ij} + S^A - Bf$$

$$F_{\sigma_{ij}} = -\frac{\delta(\Delta G)}{\delta \sigma_{ij}} = S_{ijkl} \sigma_{kl} + \alpha_{ij} \Delta T + f \bar{\epsilon}_{ij}^T$$

$\sigma_{ij}^D$  is the deviatoric part of the matrix stress tensor. These driving forces are compared with critical ones to determine the activated mechanics. Then, by considering the consistency rule ( $\dot{F}_x = \dot{F}_x^{crit}$  with  $x = f, \bar{\epsilon}_{ij}^T, T, \sigma_{ij}$ ), the constitutive law is derived in an incremental way as follows:

$$\dot{\sigma}_{ij} = L_{ijkl} \dot{\epsilon}_{kl} - M_{ij} \dot{T}$$

$L_{ijkl}$  and  $M_{ij}$  are, respectively, the mechanical and thermal tangent operators. Further details about the physical and mathematical description of the SMA phase transformation in the thermodynamical framework can be found in [21, 22].

## Actuator Simulation and Analysis

The developed actuator consists of a single SMA wire with two different zones having distinct properties in terms of responses depending on the martensite transformation. Consequently, only one SMA constitutive law has been adopted for the entire actuator's body using the same UMAT routine developed within the research group. To simulate these two different behaviors, two different initial temperatures of the actuator have been introduced in the FE model assigned to the SE and SME parts. The temperature evolution in both parts is the same and takes the memory shape temperatures as a reference for the numerical simulation. Indeed, it is worth noting that theoretically all the transition temperatures in the SME part are reached. The temperature is higher for the SE part required to bring about lower transition temperatures. The adopted transformation temperatures are summarized in Table 1. The transition temperatures for the SME part of the actuator are all reached in normal use. For this reason, the transition temperature introduced in the UMAT routine will have the same value as that for the SME. The temperature of the SE part has been increased by 46 K so that  $M_s$  reaches 325 K and corresponds to the  $M_s$  of the prototype. The fact that only one transition ( $M_s$ ) temperature is reached for the SE part indicates that this temperature must be the reference to impose the temperature difference between SE and SME parts.

Another part of the actuator that has a special importance is the transition zone between the SE and SME parts. In fact, due to the thermal processing it is difficult to know precisely the properties of this transition zone. As a consequence, a transition length of 1 mm has been set in the Finite-Element Model with elastic isotropic properties as the original NiTi austenite parameters. Thermal material parameter has been identified using DSC analyses, whereas mechanical parameters are computed from SMA wire tensile tests at several temperatures in accordance with literature [25–27].

**Table 1** Transformation temperatures adopted for the studied NiTi actuator

	SME (K)	SE (K)
$A_f$	326	280
$A_s$	313	267
$M_s$	325	279
$M_f$	312	266

In Table 2, the superscript <sup>A</sup> denotes austenite, whereas the superscript <sup>M</sup> martensite and (re) stands for the reorientation.  $E$  is the Young's modulus and  $\nu$  is the Poisson ratio of the SMA. The thermal expansion  $\alpha$  is not taken into account since the simulations are isothermal.  $H_{\min}$  and  $H_{\text{sat}}$  represent the minimal and the maximal transformation strain in the superelastic domain and  $\epsilon_{\text{max}}^{\text{re}}$  represents the maximal reorientation of martensite variants in martensite.  $K$  parameter describes the evolution of transformation strain magnitude.  $H^{\text{re}}$  is a parameter controlling hardening during reorientation and  $Y_0^{\text{re}}$  the critical stress of reorientation of martensite variants,  $b$  and  $n$  are the Prager coefficients characterizing the tension–compression asymmetry. The transformation temperatures  $M_f$ ,  $M_s$ ,  $A_s$ , and  $A_f$  are given in Table 1 and represent the martensite finish, martensite start, austenite start, and austenite finish temperatures, respectively.

In the FE software Abaqus, the boundary conditions are applied to reproduce the experimental configuration applied during the actuation as described in Sect. 2.2. and illustrated in Fig. 6.

## Results and Discussion

### Measurement of Couple as a Function of the Temperature

Thanks to the developed experimental device, it is possible to measure the angle of rotation of the actuator for different actuation temperatures. The maximum allowable rotation of the actuator with respect to the torque can be extracted from the following graph depicted in Fig. 7a.

The results presented in Fig. 7a illustrate the rotation of the actuator during thermic cycles. This experiment is carried out for several generated resistant torques. These resistant torques are induced by the SE part, the applied masses, the mechanism frictions and the fact that the transmitted rotation to the orthogonal axis is not perfect. Fig. 7a shows the hysteresis that the actuator is following as a function of the temperature. It can be noted that the

**Table 2** Material properties parameters of the NiTi actuator that are introduced into the UMAT subroutine

$E^A$ (GPa)	$E^M$ (GPa)	$n^{A,M}$	$\alpha$ ( $K^{-1}$ )	$H_{\min}$	$H_{\text{sat}}$	$K$
47	47	0.35	$1.10^{-5}$	0	0.05	0.021
$C^A$ (MPa/K)	$C^M$ (MPa/K)	$Y_0^{\text{re}}$ (MPa)	$\epsilon_{\text{max}}^{\text{re}}$	$H^{\text{re}}$	$B$	$n$
5.9	4.86	125	0.05	300	0.7	2



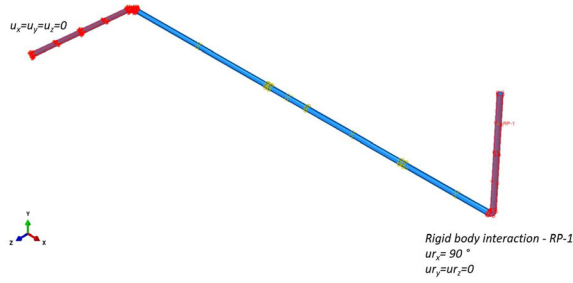


**Fig. 6** Mechanical boundary conditions applied to the torsion actuator. The left part is pinned with the 3 degrees of freedom in displacement; a rotation of  $90^\circ$  is applied in the right port with a rigid body interaction

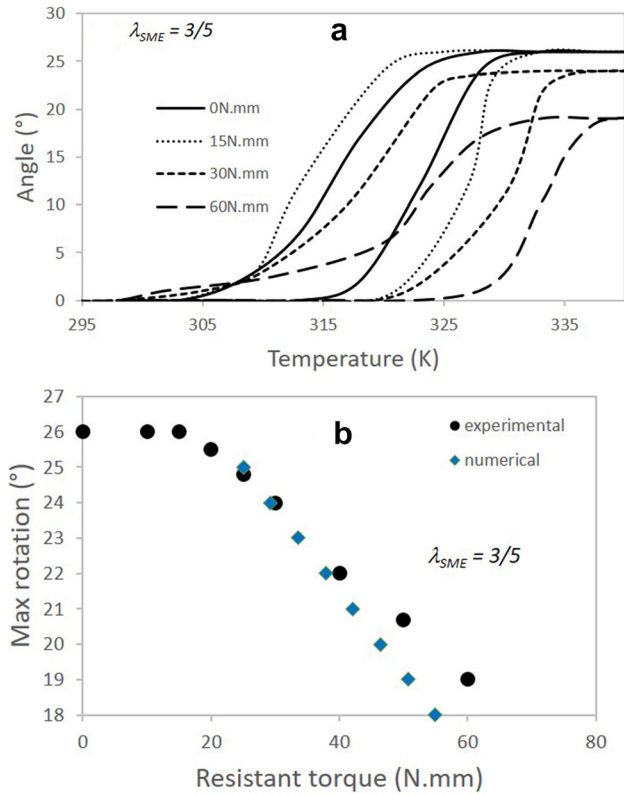


**Fig. 7** Results obtained from multi-instrumented test bench and the FE analysis: **a** Rotation of the actuator with  $\lambda_{SME}$  of  $3/5$  as a function of the temperature (heating-cooling) for different torques. One can confirm that the maximum rotation angle reached depends on the applied torque. **b** Comparison between experimental and numerical results obtained for the evolution of the maximum rotation of the studied system with respect to the resistant torque

maximum of rotation reached depends on the applied torque. In addition, one observes that the temperature range of the hysteresis depends also on the applied torque. This result highlights the influence of the imposed torque on the transformation temperatures of the actuator. A measurement of the maximal rotation induced during a thermal cycle, for several resistant torque, is presented in Fig. 7b. One can notice two phases (i) for a resistant torque below

15 Nmm, the rotation is around  $26^\circ$  which is the maximal one provided by the mechanism. For a resistant torque greater than 15 Nmm, the maximal rotation evolution is proportional to this induced torque. The comparison between experimental results and numerical predictions are discussed in the next section.

## Simulation Results and Experimental Comparison

### Comparison Between Experimental Results and FE Numerical Simulations

The FE analysis has been performed for several thermal cycles that are applied to the actuator. The position output is used in Abaqus to follow the actuator twisting according to temperature variation (heating-cooling). The model predictions are compared with the experimental findings obtained on the prototype. To this end, a FE simulation has been performed for the same range of temperatures, properties, and configuration as the experimental prototype. For the numerical estimation of the torque, the actuator has been blocked after the arming step. As a result, a response (reaction) force appears. This force can be extracted from the performed simulation. Knowing the geometry of the actuator it is easy to estimate the maximum torque of the actuator. Figure 8 represents the evolution of the generated torque as a function of the applied temperatures, during two thermal sequences (heating-cooling cycles) as detailed in Fig. 3. The result shows that the actuator achieves a maximal torque, for a configuration without any rotation, of approximately 105 Nmm.

These numerical results have been included in Fig. 7b (blue) in the range of rotation ( $18-25^\circ$ ). This value can be compared with different actuator applications that would

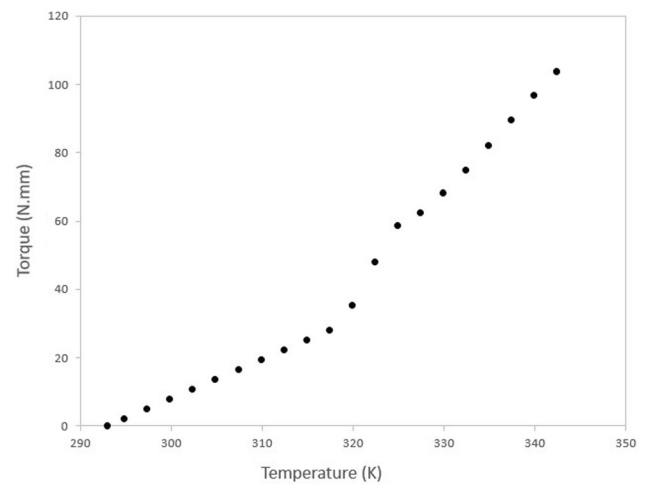


**Fig. 8** Evolution of the delivered torques with the temperature during two thermal cycles to understand how the actuator's torque is impacted by the temperature

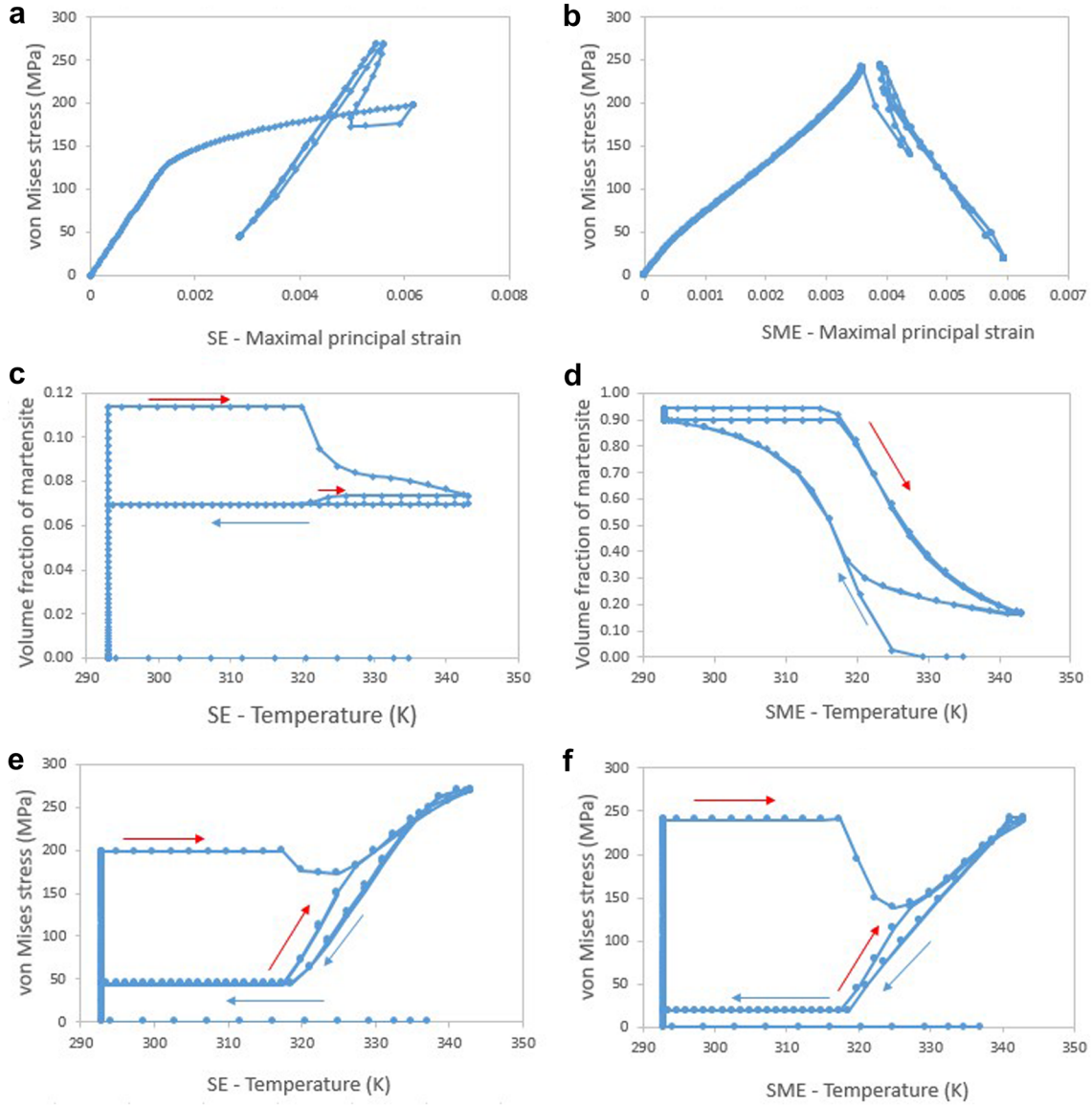


**Fig. 9** Evolution of von Mises stress with the maximal principal strain in the superelastic part (a)—Evolution of von Mises stress with the maximal principal strain in the shape memory part (b)—Evolution of Volume fraction of martensite with increments in the superelastic part (c)—Evolution of volume fraction of martensite with the applied

temperature in the shape memory part (d)—Evolution of von Mises stress with applied temperature in the superelastic part (e)—Evolution of von Mises stress with applied temperature in the shape memory part (f)

require an activation force, and with that of the experimental study. For the sake of simplicity, the Finite-Element Computation has been performed to predict the response of the actuator only in presence of the SE part as resistant part to the SME active part (rotation). Indeed, the mechanism effects as well as the induced friction and the imperfect transmission of the transmitted rotation to the welded orthogonal axis are not considered. Without any locking of the martensitic part, the maximal predicted recoverable rotation is around  $24.8^\circ$ . This value is underestimated when compared to the experimental one. Moreover, the maximal rotation decreases with respect to the applied torque according to a slope approximately of

$0.165^\circ/(\text{N/mm})$  in the experiments, whereas this decreasing slope reaches  $0.233^\circ/(\text{N/mm})$  for the numerical results.

It is established that the maximal rotation of the SMA wire is strongly dependent on the length ratio of the SME part with respect to the total length of the actuator. The effect of this length ratio ( $\lambda_{\text{SME}}$ ) is investigated in the next section.

#### *Analysis of the Martensite Volume Fraction Evolution*

It is worth noticing that the first thermal cycle only serves to assess the stresses in the actuator.

The analyses are split into two parts: the arming step and the thermal cycling. Fig. 9a) shows that a strain of 0.6% is applied to the SE part during the first arming cycle, inducing a stress of 198 MPa. The martensite volume fraction is around 11.4% at the maximal value of stress, as it is illustrated in Fig. 9c). Due to the phase transformation, the maximal stress remains lower than the plastic yield stress avoiding the occurrence of any plastic strain in the actuator. Fig. 9b) describes the evolution of the von Mises stress as a function of the applied strain in the shape memory part. The first part of the curve corresponds to the arming of the actuator generating a maximal von Mises stress of 238 MPa, and a reorientation of the martensite variants. During the first thermal cycle, it can be seen in Fig. 9a) that the volume fraction of martensite slightly decreases when the temperature reaches 320 K, inducing a diminution of stress in both SE and SME parts. During the thermal cycles, the volume fraction of the SE part evolves slightly during the cycle but remains non-significant. This shows that this part is active in the elastic regime of the biphasic alloy. The second part of the curve in Fig. 9d) corresponds to the thermal cycles applied to the actuator. It can be seen that the increase of the temperature induces a reverse phase transformation of the Shape Memory part from 91% of volume fraction of martensite to 17%. This figure confirms that the TWASE effect is correctly applied since the volume fraction of martensite reaches the value of 91% after the cooling cycle, and the SMA actuator recovers its initial shape.

Thanks to the numerical results, a distinct response of the actuator is predicted in the superelastic regime. It can be seen that after shaping, the martensite fraction no longer changes. Thus, the elasticity of this material is sufficient to reset the actuator and to bring it back to its initial position. In fact, the SE part exhibits an elastic behavior during the thermal cycles to operate the springback effect. The phase transformation only occurs during the first step of the actuation cycle (positioning, as described in Fig. 3).

This comparison confirms that the model is representative of the actuator response and can capture the different stages of its thermomechanical response.

### TWASE Actuator Optimization

The calibrated model, based on the experimental results, is then used for the optimization the actuator, especially the SME/SM ratio. Other geometries and SMAs could be investigated thanks to the model and subsequently suggest guidelines for the thermomechanical treatment of the actuator. This part is not treated in the present paper.

To identify the best length ratio  $\lambda_{SME}$ , several simulations have been carried out for different values, namely:  $\lambda_{SME} = 1/8, 1/4, 1/2, 3/5$ , and  $7/8$ . It is worth noticing that

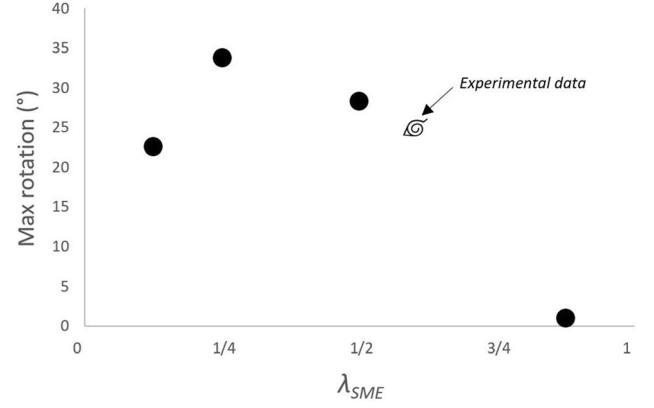


**Fig. 10** Maximum of rotation of the actuator depending upon the proportion of SME expressed through the parameter  $\lambda_{SME}$ . This can allow optimizing the maximum rotation and/or torque of the actuator

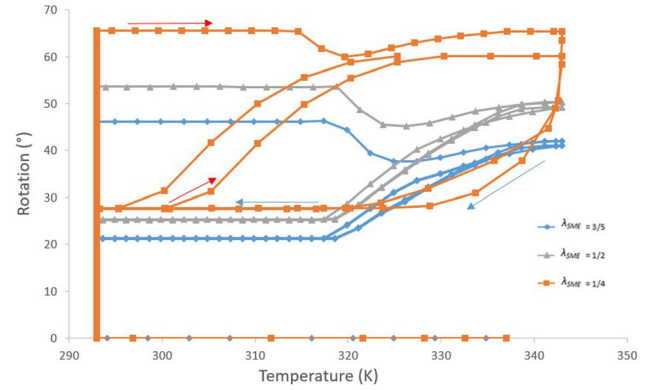


**Fig. 11** Variation of rotation angle at SE/SME interface with the temperature for three cases:  $\lambda_{SME} = 1/4$ ,  $\lambda_{SME} = 1/2$  and  $\lambda_{SME} = 3/5$

the other parameters are kept constant throughout each simulation.

Fig. 10 shows that the length ratio, which maximizes the rotation is  $\lambda_{SME} = 1/4$ . Fig. 11 describes the evolution of the rotation with the applied temperature for the 3 most interesting configurations ( $\lambda_{SME} = 1/4, 1/2$ , and  $3/5$ ).

The rotation angle induced during the arming step is strongly dependent of the length ratio. The imposed rotation of  $90^\circ$  to the extremity located close to the SME actuator part necessarily induces a greater rotation angle for the device containing only  $1/4$  of SME. During thermal cycles, the two extremities of the actuator are clamped, the rotation is totally governed by a SE and SME parts which are in opposition. Fig. 12 details the stress and strain evolution in both SME and SE parts, and the evolution of martensite fraction with the applied temperature. For each configuration corresponding to a specific  $\lambda_{SME}$ , the SME part is totally transformed between high and low temperatures, as illustrated in Fig. 12d). the actuator delivers hence the maximal value of potential rotation. These values

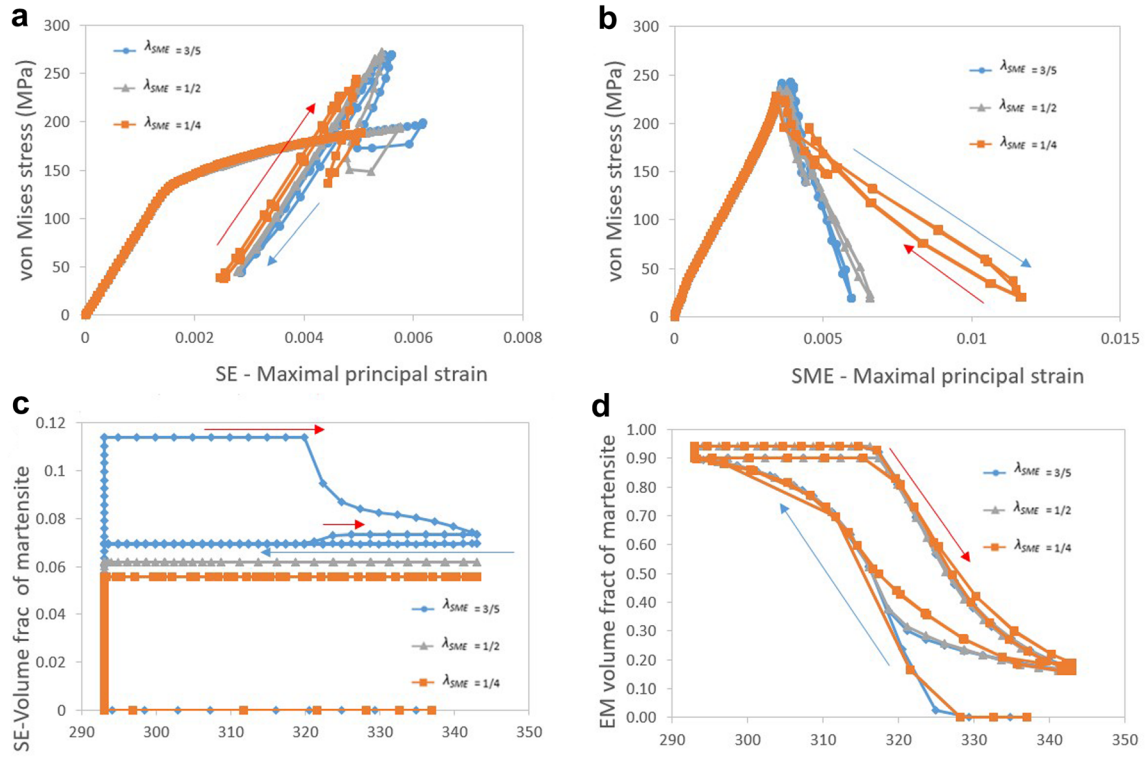


**Fig. 12** Evolution of von Mises Stress in SE (a) and SME (b) parts with maximal strain, of volume fraction of martensite in SE (c) and SME (d) parts with temperature depending on the length ratio, during

different thermal cycles—red arrows represent heating, blue arrows represent cooling (Color figure online)

**Table 3** Illustrating the value of rotation angle for the arming step and the thermal cycles

Length ratio ( $l_{SME}$ )	Rotation angle	
	Arming	Thermal cycles
1/4	68.4°	33.8°
1/2	53.6°	28.3°
3/5	46.2°	24.8°

are reached for the same temperatures, which is explained by the stress evolution during cycles that it is quite similar is SE part for the three other configurations characterized by the other values of  $\lambda_{SME}$ . However, a main difference between the three configurations can be noticed in Fig. 12b) describing the stress evolution with strain in the SME part. One can notice that in the thermal cycles, the strain evolution induced by the phase transformation has a small value around 0.2% for  $\lambda_{SME} = 1/2$  and  $\lambda_{SME} = 3/5$ , whereas this value is around 0.8% in the  $\lambda_{SME} = 1/4$  configuration. The volume of SME is smaller in this configuration but the capabilities of the phase transformation are better employed. The rotation angle in this configuration is 33.8° where it is of 28.3° for  $\lambda_{SME} = 1/2$  configuration and 24.8° for  $\lambda_{SME} = 3/5$  configuration, as shown in Table 3. In

both cases, Fig. 12c) shows that the SE part remains in elastic domain.

The  $\lambda_{SME} = 1/4$  configuration provides the best solution in terms of the delivered rotation. However, the numerical results highlight that the phase transformation is four times greater than in other configurations. This result should be taken into account for the design of applications requiring a high number of thermal cycles to avoid any degradation of SMA properties during cycling. On the contrary, for applications with low number of cycle, the simulation highlights that the maximal transformation strain is far from the maximal allowable values for NiTi. A large arming rotation leads the TWASE actuator to exhibit a large rotation angle during thermal cycle. The proposed model has the capability to model the expected response. This part devoted to the optimization of the TWASE actuator shows that different characteristics can be used to control and optimize its behavior in terms of length ratio, maximal torque, and maximal twisting angle.

## Conclusion

As a conclusion, this work has described the design and the optimization of an original SMA rotation actuator. The developed actuator is composed by a single NiTi compact



component having two distinct SMAs parts on one single axis: a superelastic part and a shape memory part. A functional prototype of this SMA autonomous actuator has been developed and fabricated to assess the feasibility of a TWASE actuator, which confers to the actuator its self-reversible response. A specific thermomechanical heat treatment has been carried out to ensure the TWASE response to the developed actuator. The latter has been experimentally and numerically analyzed through a proper prototype set-up of torsion bench. These analyses contribute to the optimization of the actuator. Using the FE analysis, the performance of the actuator has been optimized in terms of rotation angle and length ratio. The best ratio of shape memory to superelastic parts in the actuator has been predicted to 1/4 to obtain the expected two-way reversible memory effect (TWASE). The low discrepancies between the experimental results and the computational simulations can be related to the model assumptions as well as to the limitations of the experimental prototype.

As a prospect for a specific application, the developed model can be employed to optimize the maximal number of cycles (shelf life) of the TWASE actuator by limiting the maximal transformation strain as a function of geometrical parameters. The innovative self-reversible actuator developed in this work can be applied in many automotive systems that can be activated by heat transfer. Moreover, improvements can be applied in the SME and SE parts assembly thanks to the development of Additive Manufacturing technologies such as WAAM process of NiTi shape memory alloys. This could certainly increase the manufacturing efficiency considering potential industrial applications [28].

## References

- Jani JM, Leary M, Subic A, Gibson MA (2014) A review of shape memory alloy research, applications and opportunities. *Mater Des* 56:1078–1113
- Hartl DJ, Lagoudas DC (2007) Aerospace applications of shape memory alloys. *Proc Inst Mech Eng Part G* 221:535–552
- Winzek B, Schmitz S, Rumpf H, Sterzl T, Hassdorf R, Thienhaus S (2004) Recent developments in shape memory thin film technology. *Mater Sci Eng:A* 378:40–46
- Zhang C, Zee RH, Thoma PE (1996) Development of Ni-Ti based shape memory alloys for actuation and control. In: *Energy conversion engineering conference 1996 (IECEC 96)*. IEEE, pp 239–244
- Seelecke S, Müller I (2004) Shape memory alloy actuators in smart structures: Modeling and simulation. *Appl Mech Rev* 57(1):23–46
- Miková L, Medvecká-Beňová S, Kelemen M, Trebuňa F, Virgala I (2014) Application of shape memory alloy (SMA) as actuator. *Metalurgija* 54:169
- Otsuka K, Wayman CM (1998) *Shape memory materials*. Cambridge University Press, Cambridge
- Duerig TW, Melton KN, Stöcke D (1990) *Engineering aspects of shape memory alloys*. Butterworth-Heinemann Ltd., Oxford
- Chastaing K (2007) *Étude d'alliages à mémoire de forme base Ru pour applications hautes températures*. Chemical Sciences. Chimie ParisTech
- The YH, Featherstone R (2004) A new control system for fast motion control of SMA actuator wires, *Shape Memory And Related Technologies*, Singapore, 24–26 Nov 2004
- Kohl M (2010) *Shape memory microactuators (microtechnology and MEMS)*, 1st edn. Springer-Verlag, Berlin, Heidelberg
- Wada K, Liu Y (2008) On the mechanisms of two-way memory effect and stress-assisted two-way memory effect in NiTi shape memory alloy. *J Alloy Compds* 449:125–128
- Stoeckel D (1990) Shape memory actuators for automotive applications. *Mater Des* 11:302–307
- Frenzel J, George EP, Dlouhy A, Somsen C, Wagner MF, Eggeler G (2010) Influence of Ni on martensitic phase transformations in NiTi shape memory alloys. *Acta Mater* 58:3444–3458. <https://doi.org/10.1016/j.actamat.2010.02.019>
- Drexel M, Selvaduray G, Pelton A (2007) The effects of cold work and heat treatment on the properties of nitinol wire. In: *ASME 2007 2nd frontiers in biomedical devices conference*
- Oliveira JP, Shen J, Escobar JD, Salvador CAF, Schell N, Zhou N, Benafan O (2021) Laser welding of H-phase strengthened Ni-rich NiTi-20Zr high temperature shape memory alloy. *Mater Des* 202:109533
- Liu Y, Mahmud A, Kursawe F, Namb T-H (2008) Effect of pseudoelastic cycling on the Clausius-Clapeyron relation for stress-induced martensitic transformation in NiTi. *J Alloy Compds* 449:82–87
- Frenzel J, Wiczorek A, Opahle I et al (2015) On the effect of alloy composition on martensite start temperatures and latent heats in Ni – Ti-based shape memory alloys. *Acta Mater* 90:213–231. <https://doi.org/10.1016/j.actamat.2015.02.029>
- ASTM Standard (2008) Standard test method for transformation temperature of nickel-titanium alloys by thermal analysis. *Annu Book ASTM* 5:7–10
- Chemisky Y, Duval A, Patoor E, Zineb TB (2011) Constitutive model for shape memory alloys including phase transformation, martensitic reorientation and twins accommodation. *Mech Mater* 43(7):361–376
- Chatziathanasiou D, Chemisky Y, Chatzigeorgiou G, Meraghni F (2016) Modeling of coupled phase transformation and reorientation in shape memory alloys under non-proportional thermo-mechanical loading. *Int J Plast* 82:192–224
- Chatziathanasiou D, Chemisky Y, Meraghni F, Chatzigeorgiou G, Patoor E (2015) Phase transformation of anisotropic shape memory alloys: theory and validation in superelasticity. *Shape Mem Superelasticity* 1:359–374
- Chemisky Y, Hartl DJ, Meraghni F (2018) Three-dimensional constitutive model for structural and functional fatigue of shape memory alloy actuators. *Int J Fatigue* 112:263–278
- simcoon. <https://github.com/3MAH/simcoon>
- Sittner P, Heller L, Pilch J, Sedlak P, Frost M, Chemisky Y, Duval A, Piotrowski B, Zineb TB, Patoor E, Auricchio F, Morganti S, Reali A, Rio G, Favier D, Liu Y, Gibeau E, LExcellent C, Boubakar L, Hartl D, Oehler S, Lagoudas DC, Van Humbeeck J (2009) Round robin SMA modelling, *ESOMAT 2009–8th European Symposium on Martensitic Transformations*
- Meraghni F, Chemisky Y, Piotrowski B, Echchorfi R, Bourgeois N, Patoor E (2014) Parameter identification of a thermodynamic model for superelastic shape memory alloys using analytical calculation of the sensitivity matrix. *Eur J Mech A Solids* 5:226–237
- Chemisky Y, Meraghni F, Bourgeois N, Cornell S, Echchorfi R, Patoor E (2015) Analysis of the deformation paths and



thermomechanical parameter identification of a shape memory alloy using digital image correlation over heterogeneous tests. *Int J Mech Sci* 96–97:13–24

28. Ke WC, Oliveira JP, Cong BQ, Ao SS, Qi ZW, Peng B, Zeng Z (2022) Multi-layer deposition mechanism in ultra-high-frequency pulsed wire arc additive manufacturing (WAAM) of NiTi shape memory alloys. *Addit Manuf* 50:102513

**Publisher's Note** Springer Nature remains neutral with regard to jurisdictional claims in published maps and institutional affiliations.